

EXPERIMENTAL STUDY ON INFRARED PHASE-LOCKED THERMAL IMAGING INSPECTION OF CARBON FIBER REINFORCED POLYMER LAMINATES

by

**Qing-Ju TANG^{a*}, Juan JI^a, Wei-Ming FAN^a, Ling RAN^a, Si-Jie AN^a,
Tao ZHANG^a, and Chi-Wu BU^b**

^a School of Mechanical Engineering, Heilongjiang University of Science and Technology,
Harbin, China

^b School of Light Industry, Harbin University of Commerce, Harbin, China

Original scientific paper
<https://doi.org/10.2298/TSCI2202105T>

Aiming at the debonding defect of carbon fiber reinforced polymer laminates, an infrared phase-locked thermal imaging inspection system was established, and the influence of different defect diameter and depth parameters on the test was analyzed. The principal component analysis algorithm and Karhunen-Loeve Transform algorithm are used to process the image sequence, and the signal-to-noise ratio is calculated. It is concluded that principal component analysis algorithm can improve the image quality more. Gray enhancement and sharpening filter are used to improve the image clarity, thus accurately segmenting the defect features, and realize a clear and intuitive visual image.

Key words: *carbon fiber reinforced polymer laminate, infrared thermal imaging, principal component analysis algorithm*

Introduction

Carbon fiber composite is a new type of fiber material with high strength and high modulus, which contains more than 95% carbon, and has many excellent properties [1]. The axial strength and modulus of carbon fiber are high, even harder than steel. Low density, no creep, ultra-high temperature resistance in non-oxidizing environment, good fatigue resistance and good corrosion resistance; It has good electrical and thermal conductivity, good electromagnetic shielding, small thermal expansion coefficient and anisotropy, etc., and is widely used in industries, transportation, aviation, shipping and other fields [2].

Composite laminate refers to a molding process in which more than two unidirectional layers impregnated with resin are stacked, in a specified way with a specific fiber orientation to form a laminate, which is cured and molded into laminating machine under heating and pressure conditions [3]. In the manufacturing and using process of processing, there are some defects of carbon fiber reinforced polymer (CFRP) laminates: white spots, pockmarks, air gaps, delamination, debonding, surface scratches, blackening of the core, whitening around, sticking to steel plates, warping and uneven thickness [4].

Infrared thermal imaging detection technology is a new technology, which has the characteristics of non-contact, non-destructive, fast, no coupling, large area, real-time, intuiti-

* Corresponding author, e-mail: tangqingju@126.com

tive image, and so on. It is widely used in aerospace, railway track, medical treatment, machinery, petrochemical and other fields, [5-7].

Infrared phase-locked thermal imaging test

Test system

The experiment consists of halogen lamps, light modulator, infrared thermal imager, data acquisition card, and computer. Its working process is that the computer sends out sinusoidal signals, and the signals are received by the data acquisition card. The acquisition card adjusts the light modulator, and the light modulator control two halogen lamps to emit energy light waves. The infrared thermal image of CFRP laminates is obtained by the infrared thermal imager. Its working principle is shown in fig. 1.

Specimen preparation

In order to study the influence of the size and depth of defects on the experimental results, CFRP laminates with a size of 165 mm × 140 mm × 5.0 mm were prepared to simulate the debonding defects of CFRP laminates, and the specimens were laid in a single layer, ignoring the influence of the laying mode on the experiment. Schematic diagram of CFRP laminate is shown in fig. 2. and tab. 1 shows the defect size of CFRP laminates.

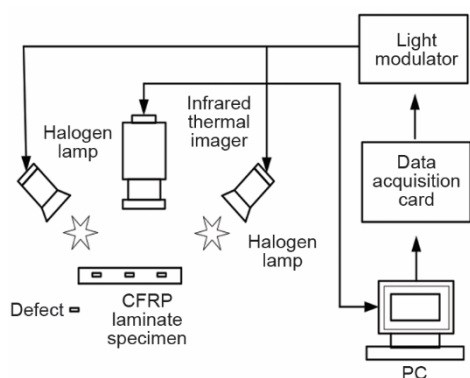


Figure 1. Infrared thermal imaging test system

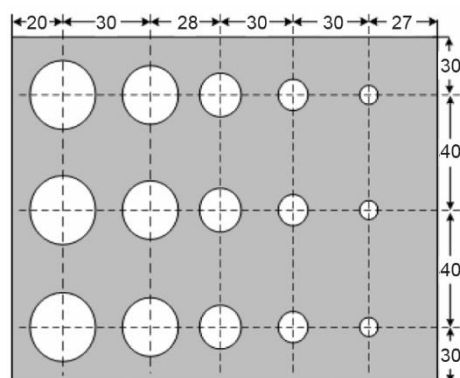


Figure 2. Schematic diagram of CFRP laminate structure

Table 1. Defect size of CFRP laminates

Row	Line	1	2	3	4	5
1		DA = 10	DA = 8	DA = 6	DA = 4	DA = 2
		DH = 3	DH = 3	DH = 3	DH = 3	DH = 3
2		DA = 10	DA = 8	DA = 6	DA = 4	DA = 2
		DH = 2	DH = 2	DH = 2	DH = 2	DH = 2
3		DA = 10	DA = 8	DA = 6	DA = 4	DA = 2
		DH = 1	DH = 1	DH = 1	DH = 1	DH = 1

where DA [mm] is the debonding diameter and DH [mm] is the debonding depth

Influence of different parameters on detection effect

The influence of defect diameter

Defect diameters of 10 mm, 8 mm, 6 mm, 4 mm, and 2 mm on the CFRP laminates were studied by selecting the most suitable output power of 2000 W, phase-locked frequency of 0.1 Hz, sampling frequency of 20 Hz and scanning time of 40 seconds.

Figure 3 is the temperature difference curve of different defect diameters. It is larger for the diameter coming out the larger amplitude, the higher temperature and the greater temperature difference, and the more obvious defect. The curve with a defect diameter of 2 mm only little changes at about 2 °C. Therefore, for CFRP laminates with the size of 165 mm × 140 mm × 5 mm, the diameter of defects that can be detected is larger than 2 mm, and the larger the diameter is, the easier it is to detect.

Defect depth

The effects of defect depth of 3 mm, 2 mm, and 1 mm on experimental results were studied by selecting the most suitable parameters, such as output power of 2000 W, phase-locked frequency of 0.1 Hz, sampling frequency of 20 Hz and scanning time of 40 seconds.

Figure 4 is a temperature difference variation curve with different defect depths. The deeper the depth, that is, the closer the distance between the defect and the surface irradiated by the light source, turning out the larger amplitude, the larger temperature difference, and the clearer defect. The temperature difference curve with a defect depth of 1 mm has a smaller amplitude and hovers between 1 °C and 2 °C. Therefore, the greater the defect depth is, the more heat reflected by CFRP laminates is, and the better the defect detection effect is. For CFRP laminates with a size of 165 mm × 140 mm × 5 mm, defects with a depth greater than 1 mm can detect the required effect.

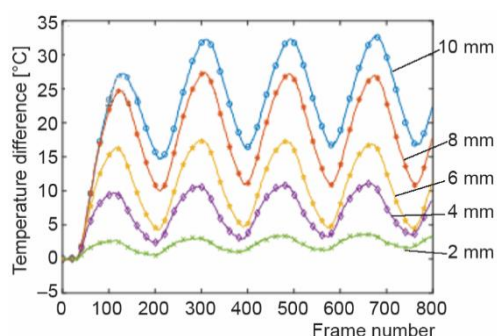


Figure 3. Frame number-temperature difference graph of different diameters

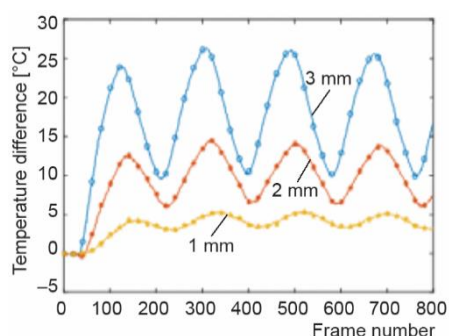


Figure 4. Frame number-temperature difference graph at different depths

Choosing CFRP laminates with proper defect diameter and depth makes the temperature difference between defect and non-defect area larger, which is convenient to identify defects, and has more important significance for subsequent research and treatment.

Image sequence processing

Theory

Principal Component Analysis Algorithm

Principal component analysis (PCA) is a mathematical method to reduce the dimension of data. Its basic idea is to try to recombine the original p indicators with certain correlation into n ($n < p$) independent comprehensive indicators to replace the original p indicators. Comprehensive index like principal component index, to the greatest extent, can not only reflect the information represented by the original variables, but also ensure that the new indexes are independent of each other. Principal component index can be expressed by:

$$F_1 = a_{11}X_1 + a_{21}X_2 + \dots + a_{p1}X_p \quad (1)$$

The amount of information extracted by each principal component can be measured by its variance. The greater the variance is, the more information the principal component index contains do. Therefore, F_1 selected from all linear combinations should be the largest variance among all linear combinations of X_1, X_2, \dots, X_p , so F_1 is called first principal component. If the first principal component is not enough to represent the information of the original p indicators, it will consider selecting the second principal component indicator F_2 . In order to reflect the original information effectively, the existing information of F_1 will not appear in F_2 , that is, F_2 and F_1 should remain independent and irrelevant, and the covariance $Cov(F_1, F_2) = 0$ is expressed in mathematical language. The F_1, F_2, \dots, F_m constructed by analogy are the first, second, ..., and m^{th} principal components of the original variable indexes X_1, X_2, \dots, X_p [8], which can be expressed by:

$$\begin{aligned} F_1 &= a_{11}X_1 + a_{12}X_2 + \dots + a_{1p}X_p \\ F_2 &= a_{21}X_1 + a_{22}X_2 + \dots + a_{2p}X_p \\ &\dots\dots\dots \\ F_m &= a_{m1}X_1 + a_{m2}X_2 + \dots + a_{mp}X_p \end{aligned} \quad (2)$$

Karhunen-Loeve transform algorithm

Given N -dimensional random variables are:

$$\bar{x} = [x_1 \quad x_2 \quad x_3 \quad \dots \quad x_n]^T \quad (3)$$

The mathematical expectation of each random variable in the vector is:

$$m_{\bar{x}} = E(\bar{x}) = (m_1, m_2, \dots, m_i, m_N)^T \quad (4)$$

Thereby the covariance of the vector is:

$$U = E[(\bar{x} - m_{\bar{x}})(\bar{x} - m_{\bar{x}})^T] \quad (5)$$

The eigenvector φ_k of the covariance matrix \mathbf{U} corresponds to its k^{th} eigenvalue λ_k , as shown in eq. (6):

$$\mathbf{U}\varphi_k = \lambda_k\varphi_k \quad \dots\dots(k = 0, \dots, N-1) \quad (6)$$

The \mathbf{U} is a symmetric matrix, so its eigenvector φ_k is orthogonal and satisfies:

$$\begin{cases} \varphi_k^T \varphi_L = 0, & (k \neq l) \\ \varphi_k^T \varphi_L \neq 0, & (k = l) \end{cases} \quad (7)$$

The unit orthogonal matrix Φ obtained after normalization is shown in eq. (8), and Satisfy the condition of eq. (9). Then N eigenvectors can be jointly expressed by eq. (10):

$$\Phi = (\varphi_0, \varphi_1, \dots, \varphi_{N-1}) \quad (8)$$

$$\Phi^T \Phi = I \quad (9)$$

$$U_\Phi = (\lambda_0 \varphi_0, \lambda_1 \varphi_1, \dots, \lambda_{N-1} \varphi_{N-1}) \quad (10)$$

Then Λ is obtained by left multiplying Φ^T on both sides of the formula (10):

$$\Phi^T U \Phi = \Lambda = \text{diag}(\lambda_0, \lambda_1, \dots, \lambda_{N-1}) \quad (11)$$

Given a 1-D random vector X , the Karhunen-Loeve (K-L) transformation of X can be defined:

$$\begin{bmatrix} y_1 \\ y_2 \\ \vdots \\ y_n \end{bmatrix} = \Phi^T \begin{bmatrix} x_1 \\ x_2 \\ \vdots \\ x_n \end{bmatrix} \quad (12)$$

That is, $Y = \Phi^T X$, and K-L transform is to project all components of X on φ_k to obtain frequency domain y_k , which changes with the change of each component in random vector \bar{x} [9].

Evaluation of processing effect of sequence algorithm

In this paper, the infrared thermograms obtained from the experiments with output power of 2000 W, phase-locked frequency of 0.1 Hz, sampling frequency of 20 Hz and scanning time of 40 seconds are processed by the infrared sequence processing methods, such as PCA and K-L. The results are shown in fig. 5. In fig. 5(a), the PCA transformation algorithm is adopted, and the carbon fiber weaving direction in the background area of the figure is quite clearly, in which the clarity degree of defects appears in different color outlines. While the defects with a diameter of 2 mm have disappeared, and the defects in the 3-D figure are obviously highlighted In fig. 5(b). The larger the diameter is, the shallower the depth of defects are, and the greater the prominence degree is. It indicates that the defects are clearer. Figure 5(c) adopts K-L transform algorithm. There are some irregular curves in the background of the figure, which shows slightly uneven terrain in the 3-D map in fig. 5(d). In the picture, all five defects with a depth of 3 mm and 2 mm appear. While only three defects with a depth of 1 mm appear, and only eight defects stand out in the three-dimensional map without obvious background noise. The defects processed by PCA algorithm are clearer, and the number of defects displayed is more than that of K-L algorithm. SNR is an important index to measure the image quality. Calculate the SNR of two algorithms and compare their processing effects.

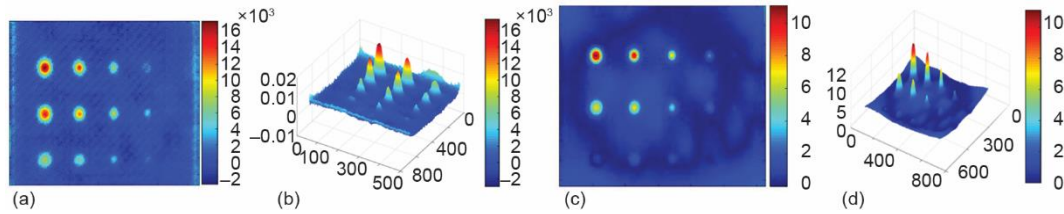


Figure 5. Processing results of different infrared sequence algorithms; (a) 2-D PCA, (b) 3-D PCA, (c) 2-D K-L, and (d) 3-D K-L (for color image see journal web site)

Normalization as shown in eq. (13) is for the convenience of data processing and the acceleration of convergence when the program runs, and limits the data to a certain range after processing. The SNR as shown in eq. (14) is a parameter for measuring image quality. In order to compare the processing effects of PCA and K-L infrared image sequence algorithms, the image is normalized firstly, then its SNR is calculated, and the SNR of each defect processed by PCA and K-L is obtained as shown in fig. 6.

Normalization can be expressed:

$$Z_n = \frac{Z - Z_{\min}}{Z_{\max} - Z_{\min}} \tag{13}$$

where Z_n is normalized data, Z , Z_{\min} , and Z_{\max} is a certain value, minimum value, and maximum value in the data, respectively.

The SNR can be expressed:

$$SNR_D = \frac{|T - R|}{\sigma^2} \tag{14}$$

where T is the average value corresponding to the defect area of the best contrast image after the original image is processed, R - the average value corresponding to the defect-free area of the best contrast image after processing the original image, and σ - the standard deviation of pixel value in the non-defective area of the best contrast image after processing the original image.

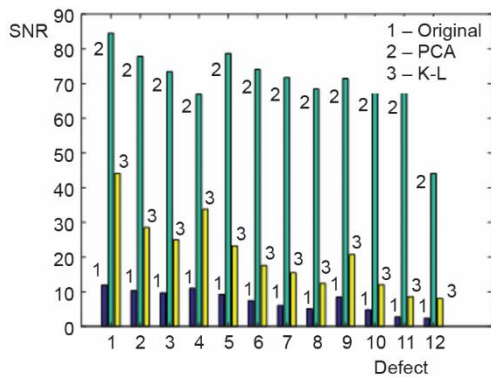


Figure 6. Comparison of image sequence processing algorithms

Figure 6 shows the SNR of the two external image sequence algorithms is calculated. From the analysis of the processing results of the infrared image sequence algorithm, it can be concluded that infrared phase-locked thermal imaging technology has a significant effect about the detection of defects in CFRP laminates with a diameter greater than 2 mm and a depth greater than 1 mm, and the PCA transform algorithm is superior to K-L transform. The defects processed by PCA algorithm can be highlighted, and the image quality is good, which provides a theoretical basis for the subsequent research and analysis.

Conclusion

In order to detect the debonding defects of CFRP laminates, an infrared phase-locked thermal imaging detection system was built. The effects of test parameters, such as defect diameter and depth, aiming at the defect detection effect of CFRP laminates were studied and discussed. The effects of PCA, K-L infrared image sequence processing were compared. The results show that, within a certain range, the larger the diameter is, the deeper the defect is, and the better the information of the defect edge can be obtained. The PCA infrared image sequence processing can not only solve the problem of uneven illumination, but also reduce noise, highlight display defects and improve image quality and SNR.

Acknowledgment

This project is supported by National Natural Science Foundation of China (Grant No. 51775175), Heilongjiang Province Natural Science Fund (Grant No. LH2021E088).

Nomenclature

T – average value of defect area, [-]
SNR – signal to noise ratio, [db]

σ – standard deviation of pixel value, [-]
 R – average value of defect free area, [-]

References

- [1] Kolobkov, A. S., et al., Development of Carbon Fiber Production Technologies A Review, *Fibre Chemistry*, 52 (2020), 1, pp. 1-5
- [2] Qin, F. V., et al., Mechanical and Electrical Properties of Carbon Fiber Composites with Incorporation of Graphene Nanoplatelets at the Fiber-Matrix Interphase, *Composites Part B*, 69 (2015), Feb., pp. 335-341
- [3] Chen, H., et al., Research Status of Carbon Fiber/Polymer Composites Based on Additive Manufacturing, *China Plastics Industry*, 47 (2019), 10, pp. 15-17
- [4] Ngo, A., et al., Nondestructive Evaluation of Defects in Carbon Fiber Reinforced Polymer (CFRP) Composites, *Nondestructive Characterization and Monitoring of Advanced Materials, Aerospace, and Civil Infrastructure* (H. Felix Wu), Society of Photo-optical Instrumentation Engineers Society of Photo-Optical Instrumentation Engineers (SPIE) Conference Series, Oregon, United States, 2017, Vol. 1, pp. 6
- [5] Vallejo, Z., J., et al., Principal Component Analysis, *Pattern Processing & Machine Intelligence Division Research Note Dra*, 1 (2012), 2, pp. 704-706
- [6] Bhairannawar, S. S., et al., FPGA Implementation of Optimized Karhunen-Loeve Transform for Image Processing Applications, *Real-Time Image Process*, 17 (2020), 6, pp. 357-370
- [7] Tian, H., Research on Robot Optimal Path Planning Method Based on Improved ant Colony Algorithm, *International Journal of Computing Science and Mathematics*, 13 (2021), 1, pp. 80-92
- [8] Huang, B. C., et al., The Recognition of Mammography Tumor Infrared Image Based on Fuzzy C-Means, (in Chinese), *Journal of Guangxi University (Natural Science Edition)*, 43 (2018), 5, pp. 1827-1835
- [9] Quintanilla-Dominguez, J., et al., Image Segmentation by Fuzzy and Possibilistic Clustering Algorithms for the Identification of Microcalcifications, *Scientia Iranica*, 18 (2011), 3, pp. 580-589